DOI: 10.15480/882.9355

Eighth International Symposium on Marine Propulsors
smp'24, Berlin, Germany, March 2024

Design and Analysis of a Pumpjet Propulsor for a Ferry Ship

Stefano Gaggero[1], Diego Villa[1], Davide Grassi[2], Federica Valdenazzi[2], Mario Felli[3], Chanwoo Bae[4]

[1] University of Genoa, Via Montallegro 1, 16145 Genoa, Italy
[2] CETENA S.p.A., Via Ippolito d'Aste 5, 16121 Genoa, Italy
[3] CNR-INM – Institute of Marine Engineering, Via di Vallerano 139, 00128, Rome, Italy
[4] BC Ferries, Victoria, British Columbia, Canada

ABSTRACT
The high efficiency of pumpjet propulsors recently favored their application to ships, different to usual high-speed vessels and submarines, to comply with the most recent regulations on efficiency, comfort onboard and noise pollution. In this context, as a part of the activity of the EU funded project SATURN, the design, and the performances of an axial pumpjet are investigated. The pumpjet of current study is designed to replace a conventional propeller of a ferry ship. To this aim a simulation-based design optimization method employing simplified RANSE analyses, synthetic wakes generated using body force distributions and a mixing-plane based coupling between rotor and stator is employed. Main geometrical characteristics (diameter, number of rotor and stator blades) as well as distributions of pitch, chord and camber are handled in the process by a parametric description of the geometry. A genetic algorithm guides towards the Pareto convergence of the designs by requiring the maximization of the propulsive efficiency at the lowest possible cavitation inception index. Fully unsteady RANSE calculations are finally employed to characterize the unsteady performances (thrust and torque) in behind conditions including the cavitation pattern and the induced pressure pulses on the ship stern, and results are discussed and compared to those of the reference conventional propeller.

Keywords
Pumpjet propulsors; Optimization; Unconventional propellers; RANSE;

1 INTRODUCTION

Pumpjet propulsors are a special case of ducted propellers combining the propeller blades and the nozzle with an additional system of stator blades that can be placed upstream or downstream of the rotating stage. In the last years, they raised lot of interests as particularly efficient propulsive systems, especially for high-speed underwater vehicles and submarines, thanks to their ability to provide high thrust under heavy loaded conditions at sensibly lower values of radiated noise. Despite early numerical studies, due to the peculiar applications of such kind of devices in the open literature there is a minimal guidance on their design, which is still mainly based on potential flow assumptions or even more simplified hydraulic analogies and charts as reviewed by Allison (1993). Some examples of design activities of this type of propulsors are those of Furuya & Chiang (1988), McCormick & Elsenhuth (1963), Kerwin et al. (1997), or Michael (2008), which, respectively, adopted blade-through and blade-to-blade flow theory, vortex theory, and iterative coupling between lifting surface methods and Euler solvers.

All these methods suffer of poor capabilities in predicting the interactions between the various components of the propulsor, which instead, may play a significant role in the case of such unconventional geometries compared to conventional propellers, for which these traditional methods were specifically developed. The action of the nozzle is typically accounted using the image method only, or by the effective velocity concept assuming asymmetric flow. The rotor/stator interaction neglects the effect of viscosity on the trailing wake of rotating blades. The leakage flow in the gap region at the tip is often heavily simplified, with consequences on the overall PJP performances.

At the same time, there are few investigations using high-fidelity numerical calculations (or experimental campaigns) on the effects of pumpjet design parameters that can guide the design process, and none of these calculations was used or was specifically planned for design purposes. Wang et al. (2020), for instance, analyzed several duct parameters, including camber, tip clearance

and angle of attack of a post-swirling pumpjet. Similar investigations were carried out by Huang et al. (2021), or Yu et al. (2020). They analyzed the influence of the duct shape, the number of stator blades, the role of chord and stagger angle. In any case, however, the number of tested configurations was quite limited to gather general guidelines, also considering that no constraints on delivered thrust or cavitation inception risk were considered during the performance comparison of the geometries, which most of the times were compared with unchanged rotor geometry. This is the context where the application of a Simulation Based Design Optimization (SBDO) approaches may represent a valid and effective alternative to old-fashioned design methods also for pumpjet propulsors. Optimization based design methods, indeed, allow using more accurate solvers like RANSE, which in the case of unconventional geometries are needed for the reliable characterization of the complex hydrodynamic phenomena these propulsors are subjected to. The application of these solvers is made possible thanks to their inclusion in a "try-and-error" process that results particularly suitable to address constrained and multi-objective designs and for the exploitation, for instance, of flow features not accountable by traditional inviscid calculations. Being the pumpjets performances a combination of the interactions of rotors, stators and nozzle, the use of a SBDO seems the natural answer to the design problem of these propulsors, addressing all the mutual influences as a whole and not simply as the (iterative) combinations of separated elements.

Current activities have been carried out in the context of the EU funded SATURN project (grant agreement No. 101006443). The SATURN project has the aim of reducing the underwater radiated noise emitted by ships and its impact on aquatic species by investigating the sources that are most harmful for marine mammals, fish and invertebrates, and by developing different mitigation solutions including pumpjet propulsions. Therefore, this paper explores the design capabilities of a RANSE based SBDO for the design of a pumpjet replacing the conventional highly-skewed propellers of a relatively fast ferry boat used as reference. At the required delivered thrust, the pumpjet is designed to maximize the efficiency and reduce the risk of cavitation. These objectives are pursued considering different combinations of number of rotor and stator blades, a variable diameter, and a parametric description of the blades (both rotor and stator) and of the nozzle to enlarge as much as possible the exploring capabilities of a metaheuristic genetic algorithm that is used to drive to convergence the design process. As a final validation of the design process, dedicated full RANSE analyses of the selected propulsor in behind ship conditions are considered to verify the outcomes and the reliability of the design process and of its necessary simplifications.

2 DESIGN CASE: THE FERRY SHIP

The test case selected for the present study is a large twin-screw ferry operated along the Canadian coast whose dimensions and particulars are listed in Table 1 and Fig. 1.

Figure 1: CAD model of the appended hull.

Table 1: Particulars of the hull.

Length	L_{PP}	156 m
Breadth	B	32.9 m
Design Draft	T	5 m
Volume at Design	V	11406 m^3
Wetted Surface at Design	S	4038 m^2

The ship hull is equipped with bulbous bow, shaft lines, V-brackets and two rudders. The geometrical features of the two original controllable pitch propellers (CPP) are illustrated in Table 2. An overview of the propellers is given in Fig. 2. The propeller is operated below the design ship speed at the design revolutions by reducing its pitch over diameter ratio (0.668 at a ship speed of 14.3 kts).

Table 2: Particulars of the propeller.

Diameter	D	3.4 m
Number of Blades	Z	4
Area Ratio	A_E/A_O	0.703
Pitch/Diameter (r/R=0.7)	$P/D_{0.7}$	1.011
Hub/Propeller radius	x_h	0.324
Direction of rotation	Inward from the top	

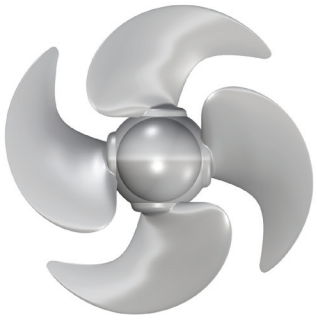

Figure 2: CAD model of the original propeller.

In order to define a coherent dataset for the PJP design, the available documentation regarding the hull and the existing propeller has been considered:

- Bare hull model test resistance curve;
- Speed and power sea trials at the design draught;
- Propeller design datasheet;

According to the sea trials, the ship top speed with the existing propeller was 20.2 kts at a reference engine power of 5531 kW whereas the propeller design speed reported on the datasheet was 21.9 kts. A reasonable estimation of the PJP design speed at the sea trial conditions is 21 kts since an increase in propulsive efficiency compared to the propeller is expected for the given engine power.

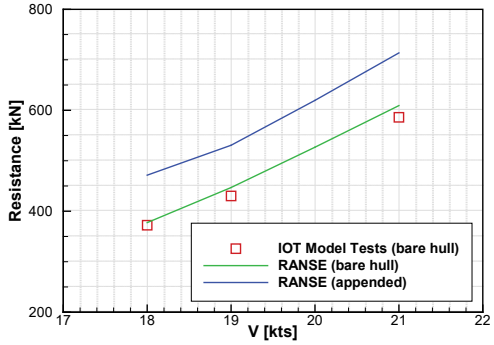

Figure 3: Predicted and measured ship resistance.

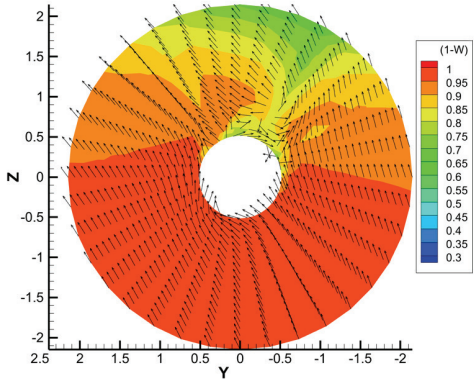

Figure 4: Computed (full scale) nominal wake at propeller disc.

When not available, dedicated RANSE analyses were employed to obtain the necessary inputs to the design process. It is the case of the required pumpjet thrust, which was derived through a preliminary RANSE computation of the bare and appended hull resistance in model scale (then extrapolated to full scale according to the ITTC'57 procedure with an allowance coefficient $C_A = 2 \cdot 10^{-4}$). Numerical results, obtained with the VoF formulation to account for the free surface and with free to trim and sink DOF to provide the dynamic attitude of the hull, are illustrated in Fig. 3 where also a comparison with the available experiments (model scale bare hull only) is given. A very good agreement is found between the numerical and experimental data. At the lowest ship speed the difference is only of 1.4%. At higher ship speeds discrepancies are never higher than 4%. The design thrust of the pumpjet is then derived at the design speed of 21 kts through the assumption of a thrust deduction coefficient (1-t) of 0.890.

Similarly, also the nominal wake at the propeller disc, which is a crucial input for the propulsor design, has been obtained by numerical calculations, in this case exploiting the double model assumption for the estimation of the full-scale hull wake (Fig. 4) by using a simpler steady calculation. Based on these data, the final design inputs for the propeller and the pumpjet are those listed in Table 3.

Table 3: Reference propeller functioning and design inputs for pumpjet.

	Propeller	Pumpjet
Ship speed [kts]	21.9	21
Nominal wake [-]	-	0.931
Shaft revolutions [RPM]	215	215
Required Thrust [kN]	-	402
Reference Power [kW]	5531	531

3 PUMPJET DESIGN

3.1 Geometry and parametric description

The pumpjet configuration considered for this activity is of "post-swirl" type, i.e., with the stator placed downstream to recover the energy losses of the rotor slipstream by straightening its wake. In this configuration, stator blades should produce and additional thrust, unloading the rotor in favor of cavitation avoidance. This geometrical configuration was preferred, moreover, for practical reasons related to the planned experimental activities at the circulation channel of INM, since with the use of a decelerating nozzle and without changing the shaft configuration of the model scale ship, the rotor/stator configuration is easier to be manufactured and managed.

In a way similar to other design activities, also for current design, a decelerating nozzle was preferred since one of the objectives of the design was on the reduction of the noise footprint of the ship, and decelerating nozzles contribute effectively for the postponement of the cavitation inception.

Design parameters were selected to provide a convenient parametric description of both the rotor and the stator blades plus the nozzle (which in current analyses was handled only by the incidence angle and its length to easily accommodate the rotor/stator) to be employed throughout the optimization process. The most relevant geometrical features of the blades determining the propulsor performances were defined by means of B-Spline curves. Due to the complexity of the design, only radial distributions of relevant geometrical features were modified, assuming for the sectional hydrofoil shape a NACA66 thickness distribution combined with a NACA a08 camber line. Stator blades were described in terms of pitch and maximum sectional camber, and assuming a constant chord value from root to tip. For rotor blades also the chord distribution was allowed to change along the blade span. A moderate, and unchanged throughout the process, distribution of skew was considered. The diameter of the rotor (consequently, of the entire propulsor) was added too to the set $\boldsymbol{x}$ of design parameters, that in the end counted 29 dimensions that represent the independent variables of the optimization problem. Regardless of the shape of rotor and stator blades, or the incidence angle of the nozzle, each pumpjet was realized with a gap (constant

from the LE to the TE of the blade) between the blade tip and the internal surface of the nozzle equal 0.5% of the rotor diameter (with reference to the rotor blade plane) and a minimum distance between trailing edge of rotor and leading edge of stator equal to 6% of the rotor diameter. The design activity, moreover, was repeated for two choices of rotor and stator blades, respectively equal to 7 rotor and 9 stator (R7/S9) or 9 rotor and 11 stator (R9/S11) blades.

3.2 Numerical models for the design activity

A computationally efficient optimization process based on RANSE requires a certain number of simplifications of the numerical model which are required to handle the calculations of thousands of different configurations. To this aim, and by exploiting some turbomachinery analogies, all the calculations relative to the optimization process (those for final verification were truly fully unsteady calculations) were realized by using the "mixing plane" concept. Instead of the fully unsteady analyses needed for time-resolved solutions of the flow across stages moving relative to one another, in correspondence of this mixing plane interface, opportunely placed between the stages, the circumferentially averaged flow field is transferred in a conservative manner between the two rotationally regions aligned on the same axis. Mass, momentum, energy, and other conserved quantities are averaged in concentric, circumferential rings of uniform radial thickness covering the entire interface boundary. Due to this averaging process, radially varying profiles of flow quantities that remain uniform along the circumferential direction within any given circumferential ring are transferred from the rotor (fore) region to the stator (aft) region, allowing for steady calculations in a sort of "equivalent" inflow. Together with periodic boundary conditions (Fig. 5), the computational domain is then reduced to a single blade passage consisting of two coaxial regions, matched by the mixing plane itself. The calculations are steady, since moving reference frame is applied in the rotor region, providing in this way a computationally efficient estimation of the averaged performances of the propulsor.

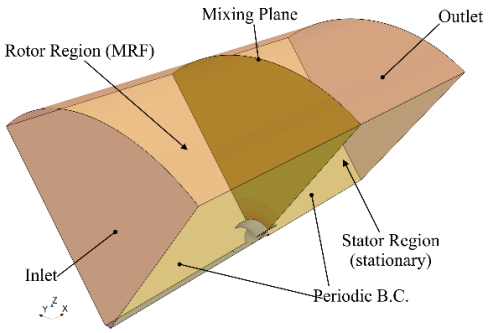

Figure 5: Computational domain for "mixing plane" analyses of the optimization process.

The adoption of a single blade passage and steady analyses prevent the possibility of designing the pumpjet propulsor accounting for the local variations of the actual ship wake, available from the preliminary RANSE analyses of the ship. Following a well-established design assumption, the design of the pumpjet blades is carried out considering, as inflow, the equivalent circumferentially averaged axial wake representative of the mean flow conditions at each blade radial position. This is in accordance with the usual design process of conventional propeller addressed using traditional lifting line-based tools. To this aim a variable velocity field has to be included into the simulations. Rather than by considering a modification of the inlet boundary condition, with all the issues related to numerical and turbulence-related dissipation, the non-uniform inflow to the propeller is obtained following the iterative methodology proposed in Baltazar et al. (2019) by using a calibrated body forces distribution placed just in front of the propeller, as per Fig. 6.

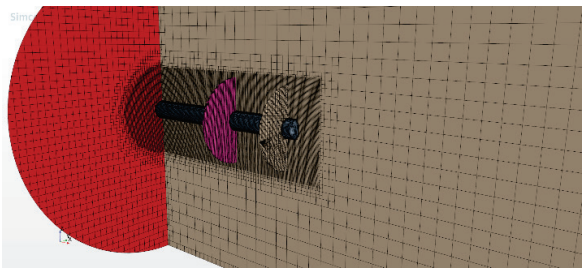

Figure 6: Body forces in front of propeller disc to reproduce the equivalent axial nominal wake.

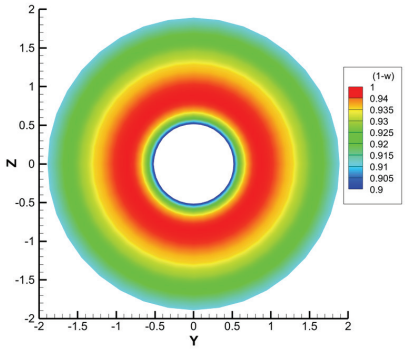

(a) Equivalent axial wake from the full-scale nominal wake;

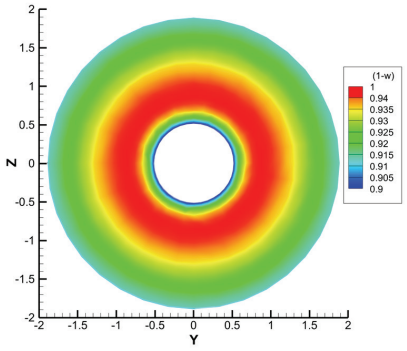

(b) Equivalent axial wake from Body Forces calibration

Figure 7: Equivalent axial wakes on the propeller disc.

By iteratively calibrating the amount of (axial) momentum added to the solution of RANS equations by the body forces, which are treated as a source term in the equations, it is possible to reconstruct the target (only axial, in this

case) radially varying, circumferentially constant, ship wake to the propeller (Fig. 7), axially equivalent to the nominal wake.

The reliability of this numerical setup was preliminary verified with a dedicated mesh sensitive analysis and some comparisons (and relative grid studies) with fully unsteady calculations in the same circumferentially averaged wake used during the design. The verification is provided for a R7/S9 configuration, but results are not qualitatively different in the case of R9/S11 geometries. All calculations use the *k-ω SST* turbulence model and second order accurate discretization schemes in space. Time dependent analyses are carried out with second order accuracy in time and an equivalent time step of 0.5 deg.

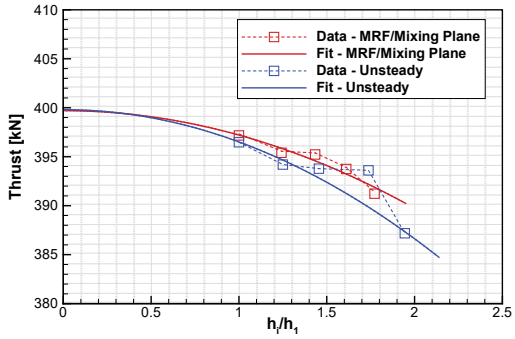

(a) Thrust

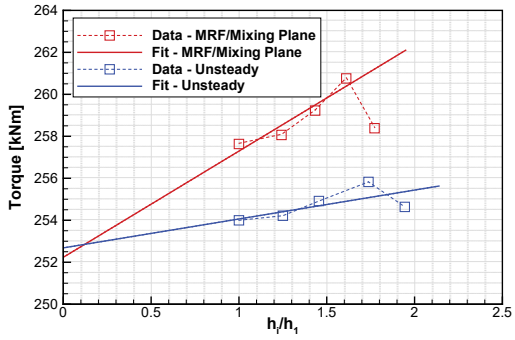

(b) Torque

Figure 8: Grid sensitivity analysis. MRF/Mixing plane calculations compared to fully unsteady analyses.

Steady calculations (blade passage, MRF and mixing plane) counted from 700k to 3.9 million cells. Corresponding unsteady analyses ranged from 4.9 to 36.5 million cells. Results of this grid sensitivity analyses are summarized in Fig. 8. The trend of thrust (both steady and unsteady calculations), evaluated with the fitting procedure proposed by Eça and Hoekstra (2014) is particularly good. The convergence is predicted of second order and compared to the extrapolated value of delivered thrust, all the meshes have negligible differences of about 1% (maximum of 2% and 3% respectively for the coarsest steady and unsteady analyses). The predicted numerical uncertainty for the mesh that can be considered the computationally affordable choice for the optimization (abt. 1.3 Million cells) is of about 4%, which is not a particularly low value but represents an acceptable compromise between the accuracy and the feasibility of calculations. Torque is a bit more problematic, since the estimated order of convergence is lower (close to 1) and the uncertainty associated with the same reference mesh is of about 8%, but with differences with respect to the extrapolated value (steady, MRF and mixing plane) lower than 3%. From these analyses, moreover, a substantial equivalence of the simplified, steady with mixing plane, model with the fully unsteady model can be observed. In terms of thrust, differences, at qualitatively similar meshes, are always lower than 1%. In the case of torque, the simplified model predicts values less than 2% different from the corresponding calculations using the fully unsteady model. These results, while confirming the reliability of the simplifications required for an affordable optimization-based design, permit to select the most appropriate mesh arrangement (abt. 1.3 million cell) shown, as an example, in Fig. 9.

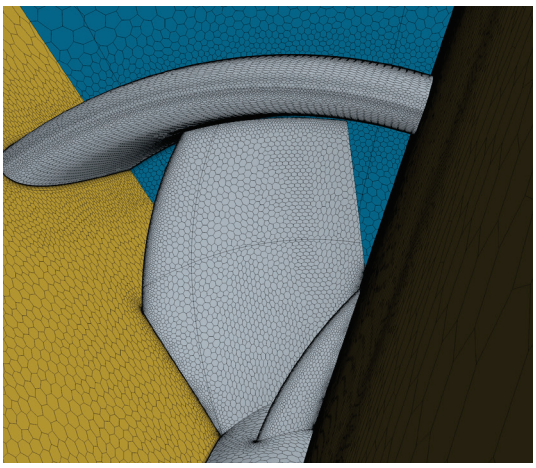

Figure 9: Reference grid (R7/S9 case) for MRF/mixing plane calculations.

3.3 Optimization process

The optimization strategy adopted for current designs is that developed for similar problems of RIM driven thrusters or Energy Saving Devices (Gaggero 2020, Furcas and Gaggero 2021). Since the computational efficiency is an unavoidable requisite for a RANSE-based optimization, non-cavitating calculations have been preferred. Rather than monitoring the portion of the rotor (or stator) blades covered by vapor, the minimization of the pumpjet cavitation has been pursued as the increase of the cavitation inception speed by monitoring the values of the pressure (C_{PN}, non-dimensional pressure coefficient using the rate of revolution), easily available through steady, non-cavitating calculations. From a mere cavitation free design, the cavitation inception has to be avoided anywhere. Then, the minimization of the highest suction peak on the entire propeller blade could be considered the only design objective of the optimization. But collecting data at different blade locations provides a more detailed characterization of the phenomena occurring on rotor and stator, which could be useful for a better understanding and for a reasoned selection of the "best" design among the Pareto configurations. To this aim, both rotor and stator blades have been subdivided in eight zones each, over

which pressure data are sampled and processed. In particular, in order to distinguish (the risk of) sheet and bubble cavitation, leading edge ($0<x/c<0.1$) and midchord ($0.1<x/c<0.6$) locations, at tip and at the root of the blades, on both back and face side of rotor and stator have been collected separately and used (with the exception of the cavitation indication of midchord root cavitation on the stator) as design objectives of the optimization process. In addition, also the extensions of the portions of the blade subjected to a pressure lower than the vapor tension (A_{CAV}) have been monitored and collected for all the configurations analyzed since the represent a further measure of the risk (and of the strength) of the possible cavitating phenomena.

In favor of computational efficiency, moreover, a continuous monitoring of the performances of any configurations has been adopted, to avoid the numerical solution up to convergence of geometries far from the required constraints. In this specific case, a loosened tolerance on the total delivered thrust (±4%) is used to accept the case as potentially feasible or to reject it and use it as a penalizing objective. Using the MOGA-II genetic algorithm (Esteco, 2017), the constrained optimization problem of Eq.1:

$$\begin{cases} maximize\ \eta_o(\boldsymbol{x}) \\ minimize\ \left(max\left(-C_{PNi}(\boldsymbol{x})\right)\right), i = 1\ldots12 \\ minimize\ \left(A_{CAVi}(\boldsymbol{x})\right), i = 1\ldots12 \\ K_{Tref} - 2\% \le K_T(\boldsymbol{x}) \le K_{Tref} + 2\% \end{cases} \quad (1)$$

is solved starting from an initial Design of Experiments, selected using Sobol sampling between the assigned range of variations of the design parameters, of 700 geometries. A total of 50 generations have been considered before collecting the most promising cases, leading to the evaluation of about 35,000 geometries per number of blade configurations.

4 RESULTS AND DISCUSSION

Some results of the optimization activities (efficiency vs. risk of cavitation inception on suction side, at the leading edge at blade tip, plus risk of suction side cavitation inception at tip, midchord, and extension of cavitating area at leading edge for the rotor, respectively through size and color of markers), are shown in Figs. 10 and 11. Overall, the R7/S9 configuration delivers better performances. At very low (lower than 2) values of risk of cavitation inception (the design cavitation index is between 1.75 and 2.25 depending on the diameter) there are geometries with predicted efficiency close to 0.69 while, in the same range of risk of cavitation, pumpjets with 9 rotor and 11 stator blades are able to provide efficiencies not higher than 0.67. A combination of all the key performance indicators, then including also possible risks of pressure side or root cavitation, plus the a-posteriori application of some thresholds on the geometric features (i.e., maximum allowable diameter) allowed the identification of a certain number of promising geometries, among which the optimal pumpjet has been selected. A collection of results of this preliminary selection is given in Fig. 12 while Table 4 summarize their performances.

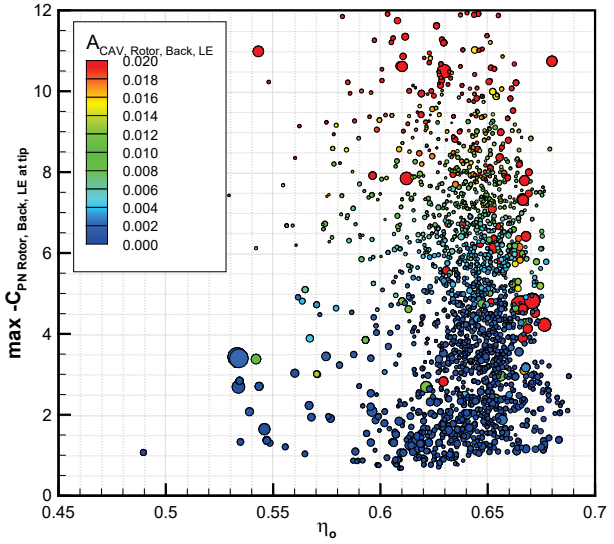

Figure 10: Pareto frontier (partial) for the R7/S9 design activity.

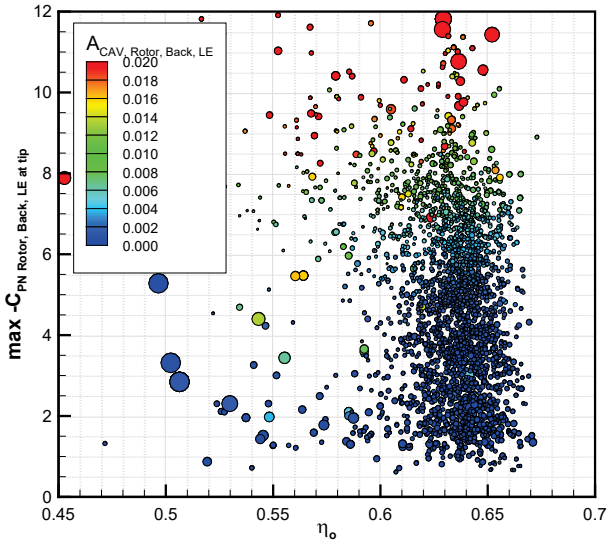

Figure 11: Pareto frontier (partial) for the R9/S11 design activity.

The optimal compromise between efficiency, cavitating performances and compact dimensions is that of R7/S9-18404. The efficiency of this geometry, at least among the solutions with a relatively small diameter, is one of the highest (0.669). The minimum value of the pressure coefficient, as predicted by the simplified model of the optimization process, is equal to about -1.9 (on the rotor blade, suction side, at the leading edge but also at midchord at the tip of the blade, in correspondence of the leakage vortex formed in the blade/nozzle gap, as barely observable in Fig.12c), which is only slightly lower than the design cavitation index of this configuration (2.22).

Pressure side cavitation, in the equivalent axial wake, is avoided everywhere on the rotor. The stator, which provides 4% of the total propulsor thrust, is completely non

cavitating, as is the nozzle, which is realized to maximize the pressure increase but, at the same time, minimize the resistance (14% of the rotor thrust).

Table 4: Summary of performances of a selection of optimal geometries.

	D [m]	T [kN]	η_o	$\sigma_{Ndes.}$
R7/S9-6073	3.11	396	0.650	2.06
R7/S9-18369	3.15	408	0.638	2.01
R7/S9-18404	3.00	406	0.669	2.22
R7/S9-20460	3.33	394	0.663	1.80
R9/S11-15613	3.04	393	0.655	2.16
R9/S11-15640	3.00	399	0.650	2.22
R9/S11-16052	3.37	393	0.664	1.76
R9/S11-18562	3.09	394	0.650	2.09

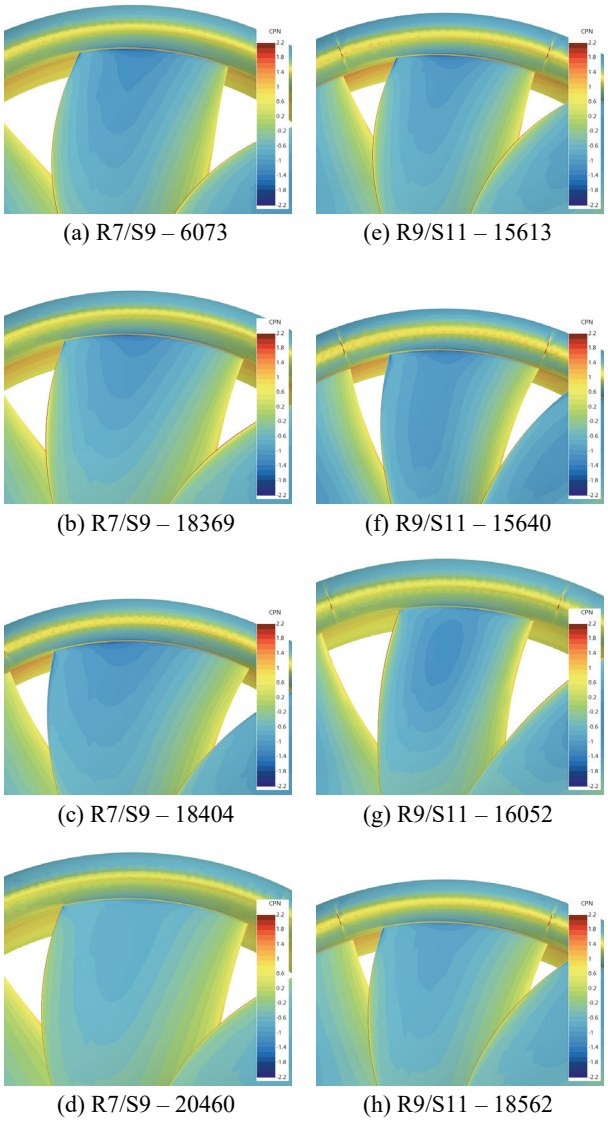

(a) R7/S9 – 6073 (e) R9/S11 – 15613

(b) R7/S9 – 18369 (f) R9/S11 – 15640

(c) R7/S9 – 18404 (g) R9/S11 – 16052

(d) R7/S9 – 20460 (h) R9/S11 – 18562

Figure 12: Pressure distributions (C_{PN}) on the suction side of a selection of optimal geometries.

The overall performances of the selected PJP have been finally assessed through a dedicated full-scale RANSE based computation campaign where the flow field around the hull and the propulsors (reference propeller and selected pumpjet) was evaluated and compared with each other and with the sea trials measurements.

4.1 Open water simulations

First, the open water wetted condition were simulated for the propeller and the PJP at different advance coefficients. The results of these computations are useful to determine the propulsive coefficients (effective wake and relative rotative efficiency) of self-propulsion calculations. The simulation of the steady flow for a single blade is possible through the application of periodic boundary conditions (similar to those already applied to the PJP during the optimization) to a propeller domain reduced to a single blade passage, having the dimensions of 3.5D (upstream), 6D (downstream) and 3D (radius). The unstructured, polyhedral grid, made of 2.6 million of volume cells is illustrated in Fig. 13, where 11 prism layers (stretch factor equal to 1.3) were located on the blades and the hub to ensure a $Y+$ distribution ranging from 30 to 150. Refinement volumes along the blade leading edge, trailing edge and tip are shown as well.

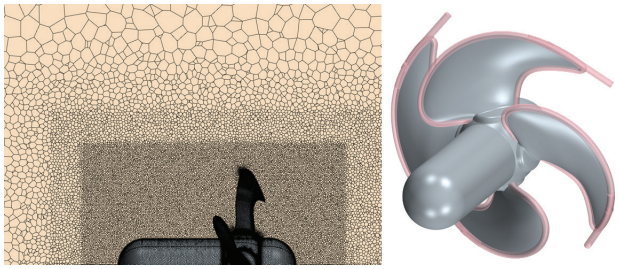

Figure 13: Grid for final open water analyses (reference propeller) and refinements regions.

As in the case of PJP optimization, the propeller rotation is simulated through the MRF (Moving Reference Frame) approach. This results in a computationally efficient steady analysis solved with the *k-ω SST* turbulence model.

Computed propeller thrust (K_T) and torque (K_Q) coefficients and open water efficiency for the design pitch over diameter ratio are summarized, as a function of the advance coefficient J, in Fig. 14.

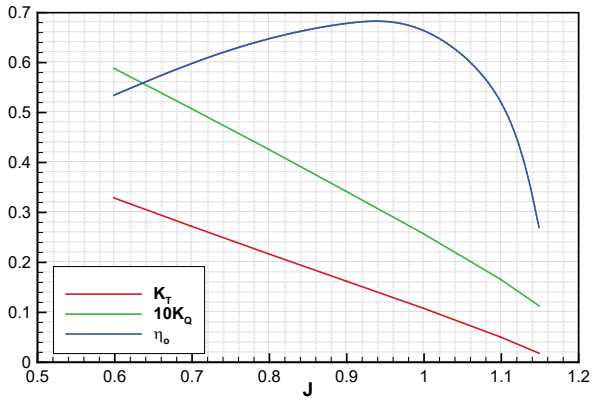

Figure 14: Computed open water curves of the reference propeller (P/D 0 1.011).

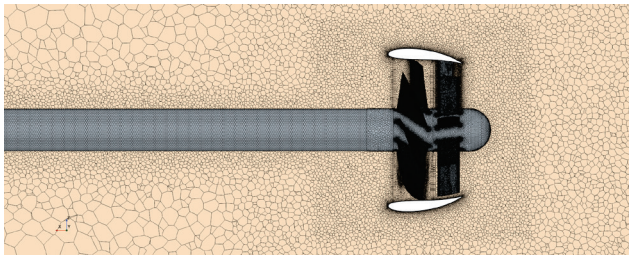

Figure 15: Grid for final open water, unsteady, analyses of the pumpjet performances.

The open water numerical model for the PJP simulation, instead, required the computation of the wetted flow field around the whole propulsor geometry through an unsteady approach, that was preferred during this final verification phase. The resulting fluid domain has the same dimensions reported for the propeller case; the rotation of the rotor is simulated by dividing the fluid domain into a stationary part (including the stator and the duct) and a rotating region containing the rotor. The interfaces between the two volume grids are managed through the Sliding Interface Approach (Fig. 15). A time step corresponding to 0.2 deg of rotor rotation was used to ensure a sufficiently low Courant number. Computed rotor, stator and duct thrust, and torque coefficients and open water efficiency are illustrated in Fig. 16.

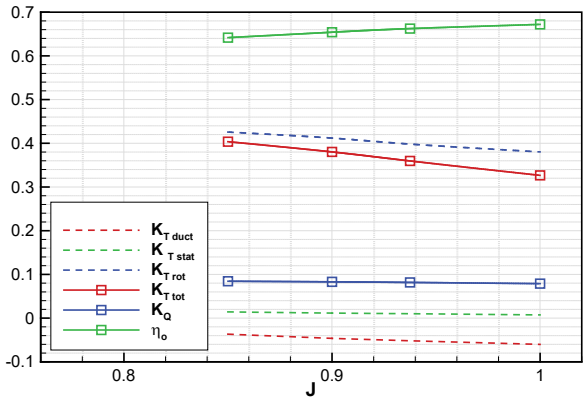

Figure 16: Computed open water curves of the selected optimized pumpjet.

4.1 In-behind condition simulations

Since the main objective of these final analyses is the characterization of the PJP and propeller performances in behind condition, the double body approach, already exploited for the calculation of the nominal wake, was adopted. In a computational domain sufficiently large to nullify the influence of the boundaries on the accuracy of the numerical results (5 L_{PP} in X, 2 L_{PP} in Y and 1 L_{PP} in Z), the free surface is replaced with a slip wall condition. This solution strategy neglects the influence of the wave pattern on the propulsors performance and allows a significant reduction in computational time. Hence, the physical model includes only two phases (liquid and vapor water) where the cavitation model is the standard Schnerr-Sauer. The rotation of the propeller (or the PJP rotor) is addressed through the Sliding Interface Approach, again by dividing the fluid domain into a stationary and a rotating region containing the propeller. A time step corresponding to 0.2 deg. of propeller rotation was used for both the propeller and PJP simulations on unstructured, polyhedral grids which counts up to 21 million of volume cells for the propeller region (12 million for the PJP rotor) and 5 million cells for the stationary region (14 million for the PJP). Details of the grids generated around the propulsors are given in Fig. 17. The turbulence model is the *k-ω SST* already used for the open water simulations. The propeller simulations were performed for three ship speeds (14.3 kts, 18 kts and 20.2 kts), fixed propeller RPM (211.4) and different pitch over diameter ratio according to the available sea trials. The PJP calculations were carried out for three ship speeds (14.3 kts, 18 kts and the design speed of 21 kts) and a rotor RPM selected in thrust identity with the propeller at the correspondent ship speed. Numerical results in terms of required shaft power for the propeller and the PJP are compared each other and with sea trials in Fig. 18 and Table 5.

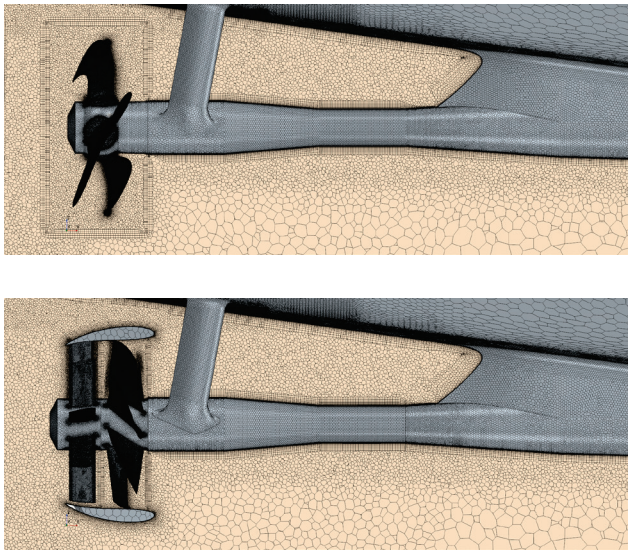

Figure 17: Arrangement of the computational grid for in-behind functioning conditions.

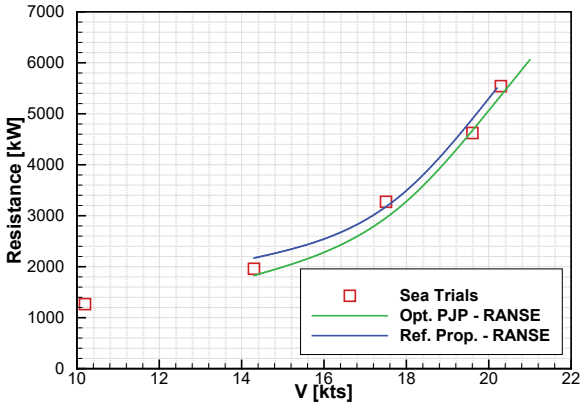

Figure 18: Estimated (sea trails, reference propeller only) and computed (reference propeller and PJP) shaft power.

A very good agreement is found between the simulations and the sea trials result thus confirming the reliability of the numerical model. The PJP shows a significant improvement in propulsive efficiency with a reduction of the required shaft power well above 4% for the whole ship

speed range considered for the analyses. An additional calculation was carried out for the PJP at the design speed of 21 kts to compare the performance in behind conditions with the outcomes of the optimization. Results are given in Table 6.

Table 5: Predicted shaft power.

Ship speed [kts]	Propeller Shaft power [kW]	PJP Shaft Power [kW]	Δ[%]
14.3	2169	1827	-15.8
18.0	3493	3280	-6.1
20.2	5503	5262	-4.4

A satisfactory agreement is found between the thrust and open water efficiency of the PJP predicted by the design procedure and by the simulations in behind condition. This confirms once more the reliability of the simplified models used for the optimization. Moreover, the effective wake computed in behind condition through a thrust identity approach with the use of the PJP open water curves (0.896) is very close to the nominal wake applied to the optimization phase (0.931).

The cavitation patterns calculated on the propeller and on the pumpjet rotor blade suction surfaces are depicted in Figure 19 for two different angular positions at the ship speed of 20.2 kts.

Table 6: Predicted thrust and efficiency for the PJP at the design speed. Comparison between equivalent inflow (optimization) and in behind condition.

	Optimization	In behind
Thrust [kN]	406	408
η_o	0.669	0.666

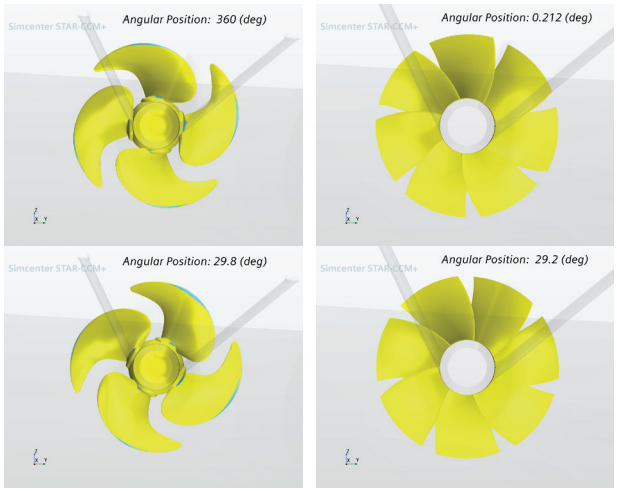

(a) Propeller suction side (b) PJ (rotor) suction side

Figure 19: Cavitation patterns on propeller and rotor suction side (nozzle hidden for readability).

The reference propeller shows a significant leading-edge sheet cavitation extended from 85% to 100% of the blade radius almost at any blade angular position. Maximum extension is reached in the 0-60 deg. rotation range, where the combined action of axial deceleration (due to the shaft brackets wake) and positive tangential velocities determines the highest angle of attack. Root cavitation at the mid-chord of the profile is observable as well. The rotor of the pumpjet, instead, is free of cavitation (both suction and pressure side), as well as the stator and the duct surfaces, which are not shown for clarity of presentation.

In order to calculate the pressure excitations on the ship, five probe points (P1-P5) were distributed on the bottom of the hull at stern, as depicted in Fig. 20. Pressure time signals were sampled for a certain number of propeller (and PJP rotor) revolutions and analyzed in the frequency domain.

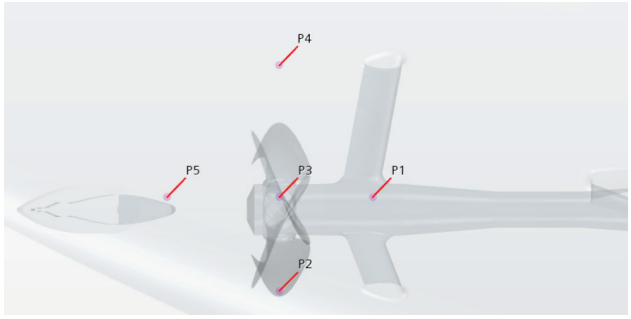

Figure 20: Pressure probes on the hull surface.

The amplitudes of the pressure pulses (as RMS) computed for the PJP and for the propeller are compared in Figs. 21 and 22 for 1st and 2nd blade harmonics respectively.

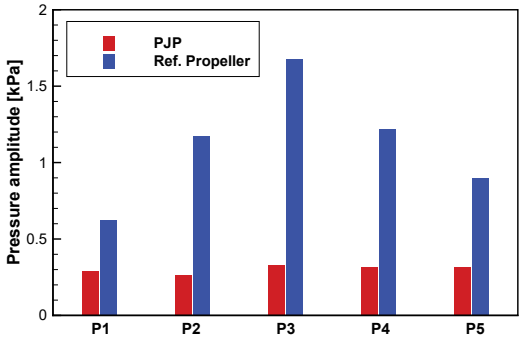

Figure 21: Pressure pulses at 1st blade passage frequency.

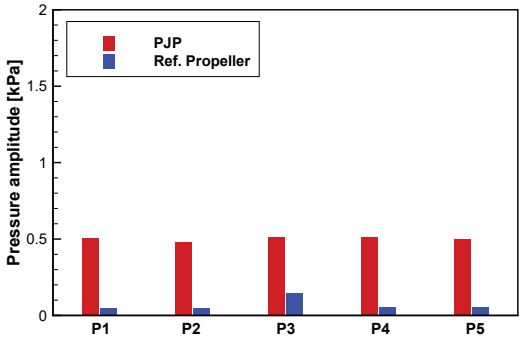

Figure 22: Pressure pulses at 2nd blade passage frequency.

Compared to the reference propeller, the pumpjet provides a substantial reduction of the pressure pulses amplitudes, at least for what regards the 1st blade passage, at any sampling point locations. This improvement can be related to different phenomena: the "shielding" effect of the nozzle

(that has its maximum influence for the points just above the propulsor) but also the suppression of the cavitation, observable for the probing points in the wake (P5) or in front (P1) of the propeller/pumpjet. On the contrary, the pumpjet shows a significant content (even if much smaller that the 1st) at the 2nd blade frequency, which results always higher than the reference propeller.

5 CONCLUSIONS

The design of a pumpjet propulsor for a ferry ship has been addressed using a simulation-based design optimization method combining a parametric description of the geometry, a RANSE solver, and a genetic optimization algorithm. The geometry is described thanks to B-Spline curves representing the most influential radial quantities (pitch, camber, chord) of both rotor and stator blades. A decelerating nozzle is employed, since the focus is on the reduction of cavitation occurrence. RANSE analyses are carried out exploiting a simplified numerical setup (mixing plane, periodic boundary conditions and equivalent axial wake inflow by an appropriate body forces distribution) to permit the analysis of thousands of different configurations (up to 35,000) in a reasonable design time. The results of the design activity show a satisfactory (within the accepted simplifications) reduction of the risk of cavitation and promising values of propulsive efficiency, especially for the 7 rotor/9 stator blades configurations, despite the presence of a decelerating nozzle and its additional drag. For the current application, a rotor/stator configuration using 7 rotor blades and 9 stator blades is finally selected as the most promising and its performances are systematically compared, also in behind ship conditions, to those of the reference conventional propeller.

To this aim, a dedicated CFD campaign, switching from steady equivalent to fully unsteady RANSE calculations on very refined computational grids (more than 25 million cells), has been carried out. Results in terms of total thrust, efficiency and wake fraction demonstrate the reliability and robustness of the simplified design procedure. The same numerical model is applied to assess the flow field around the existing reference propeller. The main outcomes of this analysis indicate a clear advantage of the pumpjet propulsor in terms of required power (at a given ship speed), cavitation extension on the blade/rotor surface and related pressure pulses amplitude over the hull surface. The use of the optimized pumpjet ensures a substantial reduction of the required power (4% at the design speed, higher than 6% at lower ship speeds) together with an almost complete avoidance of cavitation on the rotor blades. Induced pressure pulses (1st harmonic) are more than halved and only negligible 2nd order harmonics (not present in the case of the conventional propeller), in any case well below acceptable limits, are observed.

REFERENCES

Allison, J.L. (1993). 'Marine waterjet propulsion'. Trans. Of SNAME, **101**, pp. 275-335.

Baltazar, J., Schuiling, B., & Rijpkema, D. (2019). 'Propeller Performance Prediction in an Artificially Generated Wake Field Using RANSE', 22nd Numerical Towing Tank Symposium, Tomar, Portugal.

Eça, L., & Hoekstra, M. (2014). 'A procedure for the estimation of the numerical uncertainty of CFD calculations based on grid refinement studies'. Journal of computational physics, 262, 104-130.

Esteco (2017). modeFRONTIER Users' Manual.

Furcas, F., & Gaggero, S. (2021). 'Pre-swirl stators design using a coupled BEM-RANSE approach'. Ocean Engineering, **222**, 108579.

Furuya, O., & Chiang, W. L. (1988). 'A new pumpjet design theory'. DTIC Document.

Gaggero, S. (2020). 'Numerical design of a RIM-driven thruster using a RANS-based optimization approach'. Applied Ocean Research, **94**, 101941.

Huang, Q., Li, H., Pan, G., & Dong, X. (2021). 'Effects of duct parameter on pump-jet propulsor unsteady hydrodynamic performance'. Ocean Engineering, **221**, 108509.

Kerwin, J. E., Taylor, T. E., Black, S. D., and McHugh, G. P. (1997). 'A coupled lifting-surface analysis technique for marine propulsors in steady flow'. SNAME Propellers/Shafting '97 Symposium,Virginia Beach, VA.

McCormick, B. W., & Elsenhuth, J. J. (1963). 'Design and performance of propellers and pumpjets for underwater propulsion'. AIAA Journal, **1**(10), 2348-2354.

Michael, T. J., Schroeder, S. D., & Becnel, A. J. (2008). 'Design of the ONR AxWJ-2 axial flow water jet pump'. Naval Surface Warfare Center Carderock Division, Report NSWCCD-50-TR-2008/066

Siemens, P.L.M. (2020). StarCCM+ Users' Manual, V. 15.06. Siemens PLM.

Wang, C., Weng, K., Guo, C., Chang, X., & Gu, L. (2020). 'Analysis of influence of duct geometrical parameters on pump jet propulsor hydrodynamic performance'. Journal of Marine Science and Technology, **25**(2), 640-657.

Yu, H., Duan, N., Hua, H., & Zhang, Z. (2020). 'Propulsion performance and unsteady forces of a pump-jet propulsor with different pre-swirl stator parameters'. Applied Ocean Research, **100**, 102184.